Frontiers of Information Technology & Electronic Engineering
www.jzus.zju.edu.cn; engineering.cae.cn; www.springerlink.com
ISSN 2095-9184 (print); ISSN 2095-9230 (online)
E-mail: jzus@zju.edu.cn

Correspondence:

Miniaturized diplexer with wide-stopband based on half-mode substrate integrated waveguide*

Ziyu ZHOU, Gang DONG‡, Xinqing LEI, Zhangming ZHU

School of Microelectronics, Xidian University, Xi'an 710071, China

E-mail: 22111110508@stu.xidian.edu.cn; gdong@xidian.edu.cn; 23111110115@stu.xidian.edu.cn; zmyh@263.net

Received Oct. 24, 2024; Revision accepted Jan. 24, 2025; Crosschecked July 1, 2025

https://doi.org/10.1631/FITEE.2400944

A miniaturized diplexer with a wide-stopband based on half-mode substrate integrated waveguide (HMSIW) is proposed. The diplexer combines a dual-mode resonator (DMR) with single-mode resonators (SMRs). The employment of HMSIW technology breaks through the limitations of SMRs on miniaturization, while effectively addressing the limitation on wide-stopband performance that is typically encountered with the TE_{202} mode in the SMRs. A second-order prototype, centered at 10.34 GHz and 13.90 GHz, has been designed and fabricated, using a TE_{101}/TE_{301} DMR. The measured out-of-band rejection is better than 20 dB with a frequency of up to $2.16f_1$ (f_1 is the center frequency of channel 1). Meanwhile, the size of the diplexer is reduced to $1.363\lambda_g^2$ (λ_g is the guided wavelength in the dielectric substrate at f_1).

1 Introduction

As a special type of filter, diplexers separate the transmission and reception channels of a common antenna. Due to the significant impact on wireless communication systems, the trend in diplexer design focuses on wide-stopband performance, high isolation, low insertion loss, and miniaturization (Bavandpour et al., 2021; Roshani et al., 2023). Substrate integrated waveguide (SIW) technology has become an effective solution for diplexer designs as it provides high Q and electromagnetic interference shielding while significantly reducing the size.

In a conventional design, T-junctions are used in diplexers to separate two passbands (Sirci et al., 2015). Many studies aim to minimize the circuit size by eliminating T-junctions. A compact diplexer has been proposed (Cheng et al., 2013), using multiple DMR connections, which cannot control the bandwidth of two channels separately. Another approach integrates DMR and SMRs within a diplexer to independently control the bandwidth of each passband, establishing a classic topology (Zhou et al., 2018a). However, this topology still incorporates multiple SMRs, which occupy a significant amount of space and hinder further miniaturization. Alternative miniaturization methods have been proposed, such as multi-layer stacking technology (Iqbal et al., 2019), HMSIW (Zhou and Wu, 2021), and folded SIW (Sieganschin et al., 2021). Nevertheless, both multi-layer technology and folded SIW increase the design complexity and manufacturing costs.

The stopband characteristic is also one of the key performances of diplexers, as the wide-stopband can effectively reduce the external or internal signal interference. However, designing compact SIW diplexers with a wide-stopband remains a challenge.

‡ Corresponding author

* Project supported by the National Natural Science Foundation of China (Nos. U23A20291 and 62021004) and the National Key Research and Development Program of China (No. 2023YFF0616600)

ORCID: Gang DONG, https://orcid.org/0000-0001-6557-2286

Building on the topology that combines DMR and SMRs, various techniques have been implemented to achieve wide-stopband SIW diplexers without T-junctions, such as the harmonic staggered technique (Zhou et al., 2020), orthogonal transmission (Xie et al., 2020), and center-coupled windows (Ma et al., 2023). However, in these studies, since the TE_{202} mode in the SMRs is not completely suppressed, the boundary of the stopband is limited to around $2f_1$.

In this study, a compact and wide-stopband SIW diplexer is proposed, based on the HMSIW technology. Using half-mode substrate integrated rectangular cavities (HMSIRCs) as DMR and SMRs overcomes the limitations of SMRs on the miniaturization and wide-stopband performance. The TE_{202} mode is effectively eliminated from SMRs as the specific even modes in HMSIRC are not excited due to magnetic walls in the symmetry plane (Lai et al., 2009). The TE_{102} mode is suppressed, elevating TE_{301} as the first unsuppressed mode in SMRs. Therefore, the diplexer can obtain a wider stopband only through second-order resonance. The usage of HMSIRCs, coupled with a reduced number of resonators, further minimizes the circuit size. A second-order prototype based on TE_{101}/TE_{301} DMR is designed and fabricated, covering a wide range of frequency ratios. Measurements show that the prototype exhibits excellent stopband performance with a small size.

2 Realization method of dual-band and wide-stopband

In the proposed diplexer, the first two modes in the DMR and the first mode in the SMRs form two passbands. To achieve dual-band and wide-stopband, the higher-order mode characteristics of HMSIRC are analyzed. Substrate integrated rectangular cavity (SIRC), as an equivalent structure of HMSIRC, has dimensions denoted by W and L in the x- and z-axis directions, respectively ($W \geq L$). If we define f_1^{r}, f_2^{r}, and f_3^{r} as the resonant frequencies of the first three modes, we can obtain $f_1^{\mathrm{r}} = f_{\mathrm{TE101}}$. Normalized frequency ratios k_{m0q} are used to analyze higher-order distributions, which can be deduced using Eq. (1) (Zhou et al., 2017):

$$k_{m0q} = \frac{f_{\mathrm{TE}m0q}}{f_{\mathrm{TE101}}} = \sqrt{q^2 + \frac{m^2 - q^2}{1 + (W/L)^2}}, \quad (1)$$

where m and q are the mode indices along the x- and z-axis directions, respectively. Considering the removed modes TE_{201} and TE_{202}, the higher-order mode distributions in HMSIRC can be divided into three main cases based on the W/L ratio, as shown in Table 1. We can deduce that the realizable range of $f_2^{\mathrm{r}}/f_1^{\mathrm{r}}$ is [1, 1.784] when the second mode in HMSIRC is TE_{301}. Therefore, DMR is designed with $f_1^{\mathrm{r}}=f_{\mathrm{TE101}}$ and $f_2^{\mathrm{r}}=f_{\mathrm{TE301}}$ to achieve a wide range of realizable frequency ratios.

Table 1 Cases of higher-order mode characteristics of half-mode substrate-integrated rectangular cavity (HMSIRC) with different W/L values

	Case 1 [1, 1.633)	Case 2 [1.633, 2.828)	Case 3 [2.828, $+\infty$)
1st mode	TE_{101}	TE_{101}	TE_{101}
2nd mode	TE_{102}	TE_{301}	TE_{301}
3rd mode	TE_{301}	TE_{102}	TE_{501}
$f_2^{\mathrm{r}}/f_1^{\mathrm{r}}$	[1.581, 1.784]	[1.374, 1.784]	(1, 1.374]
$f_3^{\mathrm{r}}/f_1^{\mathrm{r}}$	[1.784, 2.236]	[1.172, 1.837]	(1, 1.914]

To achieve wide-stopband, the third mode in DMR and the second mode in SMRs should be suppressed by strategically positioning the internal coupling windows within the regions of the weakest electric field for each respective mode. The electric field magnitude distributions of the TE_{101}, TE_{102}, and TE_{301} modes in an HMSIRC and their suppression positions are shown in Fig. 1. The internal coupling window for the HMSIRC should be set at half of the common post-wall along the z axis if the TE_{102} mode is to be suppressed. If the TE_{301} mode is to be suppressed, the internal coupling window should be set at one-third of the common post-wall along the x axis. From Table 1, it can be concluded that the values of $f_2^{\mathrm{r}}/f_1^{\mathrm{r}}$ and $f_3^{\mathrm{r}}/f_1^{\mathrm{r}}$ increase as W/L decreases. W/L of SMRs is designed to be close to 1 to stagger the higher-order modes in DMR and SMRs.

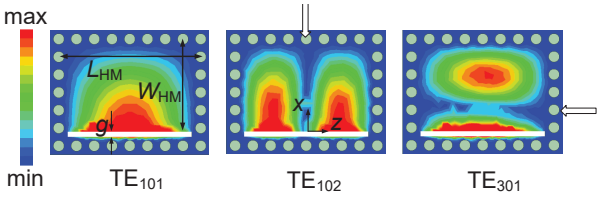

Fig. 1 Electric field magnitude distributions of TE_{101}, TE_{102}, and TE_{301} modes in a half-mode substrate-integrated rectangular cavity (HMSIRC). W_{HM} and L_{HM} denote the width and length of the HMSIRC respectively, and g is the width of the gap on the metal layer

Therefore, the second mode in SMRs is the TE_{102} mode. Due to the inhibition of the TE_{102} mode in SMRs, the first unsuppressed mode in SMRs is the TE_{301} mode, which specifies the stopband boundary of the diplexer. Consequently, the stopband of the proposed diplexer can be extended to $2.236f_1$ at most. For whole mode SMRs with the same W/L value, TE_{202} is the first unsuppressed mode, thus achieving a maximum stopband of $2f_1$ for the diplexer.

3 Synthesis and design of wide-stopband diplexer based on HMSIW

3.1 Coupling topology

Fig. 2a depicts the coupling topology of the second-order prototype. HMSIRC 1 operates with the TE_{101} resonance at f_1 and the TE_{301} resonance at f_2, while HMSIRC 2^{I} and 2^{II} operate with TE_{101} resonances at f_1 and f_2, respectively. The configuration of the proposed diplexer is shown in Fig. 2b. It can be seen that input port 1 is set to offset t_{i} to control the external couplings of the two modes for flexible control of the dual bandwidth. The internal coupling window between HMSIRC 1 and 2^{I} rejects the TE_{102} mode in HMSIRC 2^{I}. Additionally, the internal coupling window between HMSIRC 1 and 2^{II} rejects the TE_{102} mode in HMSIRC 2^{II}.

3.2 Design parameters and FBW design graph

This second-order diplexer is synthesized according to the conventional Chebyshev prototype filter with a return loss (RL) of around 20 dB. The element values of the corresponding low-pass prototype filter can be found as $g_0^{\mathrm{I,II}}=1$, $g_1^{\mathrm{I,II}}=0.6648$, $g_2^{\mathrm{I,II}}=0.5445$, $g_3^{\mathrm{I,II}}=1.2210$ (Hong and Lancaster, 2004). The diplexer is designed and fabricated on the Rogers RT/Duroid 3003 substrate (dielectric constant $\varepsilon_{\mathrm{r}}=3$, thickness $h=0.508$ mm, and loss tangent $\tan\delta=0.001$). The diameter (d) of metallized via-holes and the distance (p) between the adjacent via-holes in the cavity are 0.6 mm and 1 mm, respectively. The physical sizes of the HMSIRCs can be calculated using Eqs. (2)–(4) (Zhou et al., 2018b):

$$W_{\mathrm{HMSIRC}}=W_{\mathrm{SIRC}}/2-\Delta W, \tag{2}$$

$$L_{\mathrm{HMSIRC}}=L_{\mathrm{SIRC}}, \tag{3}$$

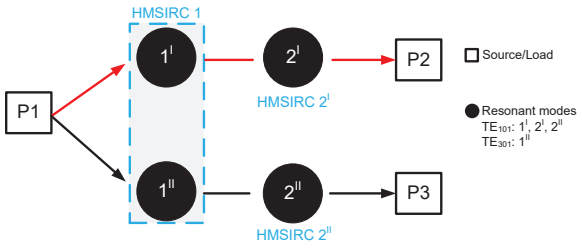

(a)

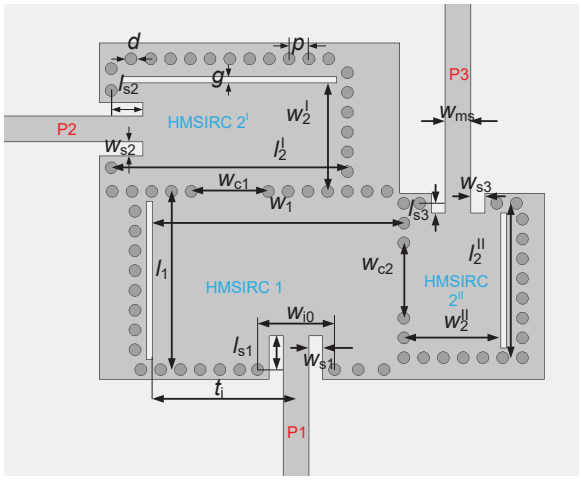

(b)

Fig. 2 Proposed SIW diplexer based on HMSIRCs: (a) coupling topology; (b) geometric configuration. $w_2^{\mathrm{I}}/w_2^{\mathrm{II}}$ and $l_2^{\mathrm{I}}/l_2^{\mathrm{II}}$ are the width and length of HMSIRC 2^{I} and 2^{II}, respectively. P1, P2, and P3 represent ports 1, 2, and 3 of the diplexer, respectively. $w_{\mathrm{s1}}/w_{\mathrm{s2}}/w_{\mathrm{s3}}$ and $l_{\mathrm{s1}}/l_{\mathrm{s2}}/l_{\mathrm{s3}}$ are the width and length of the two gaps of feeding ports 1, 2, and 3, respectively. t_{i} refers to the distance between feeding port 1 and the gap in HMSIRC 1. $w_{\mathrm{c1}}/w_{\mathrm{c2}}$ is the coupling window width of HMSIRC 2^{I} and 2^{II}, respectively. w_{ms} is the width of the feeding microstrip line. w_{i0} is the width of the feeding port

$$\frac{\Delta W}{h}=\left(0.05+\frac{0.03}{\varepsilon_{\mathrm{r}}}\right)\ln\left(0.79\frac{(W/2)^2}{h^3}+\frac{104(W/2)-261}{h^2}+\frac{38}{h}+2.77\right), \tag{4}$$

where W_{HMSIRC} and L_{HMSIRC} represent the width and length of the HMSIRC, and W_{SIRC} and L_{SIRC} represent the width and length of the corresponding SIRC, respectively. ΔW describes the effect of fringing fields on the open boundary of HMSIRC (Zhou et al., 2018b). In addition, ε_{r} is the relative permittivity. The initial size of HMSIRC 1 can be calculated with $f_1=f_{\mathrm{TE101}}=10.34$ GHz and $f_2=f_{\mathrm{TE301}}=13.90$ GHz. The fractional bandwidths (FBWs) of the lower and upper channel filters (Δ_1 and Δ_2) can

be obtained as

$$\begin{cases} \Delta_1 = g_0^{\mathrm{I}} g_1^{\mathrm{I}} / Q_{\mathrm{e}}^{\mathrm{I}} = M_{12}^{\mathrm{I}} \sqrt{g_1^{\mathrm{I}} g_2^{\mathrm{I}}}, \\ \Delta_2 = g_0^{\mathrm{II}} g_1^{\mathrm{II}} / Q_{\mathrm{e}}^{\mathrm{II}} = M_{12}^{\mathrm{II}} \sqrt{g_1^{\mathrm{II}} g_2^{\mathrm{II}}}, \end{cases} \tag{5}$$

where $Q_{\mathrm{e}}^{\mathrm{I,II}}$ is the external quality factor of two passbands, and can be easily calculated as

$$Q_{\mathrm{e}}^{\mathrm{I,II}} = \frac{2\pi f_0^{\mathrm{I,II}} \tau_{S_{11}}(f_0^{\mathrm{I,II}})}{4}. \tag{6}$$

Here, $f_0^{\mathrm{I,II}}$ is the resonant frequency of TE_{101} and TE_{201} modes, and $\tau_{S_{11}}(f_0^{\mathrm{I,II}})$ is the group delay of S_{11} at $f_0^{\mathrm{I,II}}$.

$M_{12}^{\mathrm{I,II}}$ is the internal coupling coefficient in two channels, which can easily be extracted by

$$M_{12}^{\mathrm{I,II}} = \left(\frac{f_{\mathrm{H}}^2 - f_{\mathrm{L}}^2}{f_{\mathrm{H}}^2 + f_{\mathrm{L}}^2} \right)^{\mathrm{I,II}}, \tag{7}$$

where f_{H} and f_{L} are the higher and lower resonant frequencies, respectively.

According to Eq. (5), if the diplexer is established with $\Delta_1 = 2.14\%$ and $\Delta_2 = 2.15\%$, the theoretical Q_{e} of two passbands can be determined as $Q_{\mathrm{e}}^{\mathrm{I}}$=31.06 and $Q_{\mathrm{e}}^{\mathrm{II}} = 30.92$. Then the corresponding coupling matrices of the two channels can be obtained according to Eq. (5):

$$[M]^{\mathrm{I}} = \begin{bmatrix} 0 & 0.0355 \\ 0.0355 & 0 \end{bmatrix}, \tag{8}$$

$$[M]^{\mathrm{II}} = \begin{bmatrix} 0 & 0.0375 \\ 0.0375 & 0 \end{bmatrix}. \tag{9}$$

Hence, with the given design bandwidths of the lower and upper channel filters, we can separately determine the size of the coupling windows and the coupling degree of the output port for filters of each channel. Meanwhile, the dimension of the common input port P1 needs to be designed according to the bandwidth requirements of two channels. Fig. 3 shows the available FBWs of the two channels against the offset t_{i} and the length of the input port l_{s1} with fixed $w_{\mathrm{ms}} = 1.29$ mm, $w_{\mathrm{s}} = 0.7$ mm, and $w_{\mathrm{i0}} = 3.9$ mm. According to the FBW design graph, when the diplexer is established with $\Delta_1 = 2.14\%$ and $\Delta_2 = 2.15\%$, the parameters of the input port are displayed by point P as $t_{\mathrm{i}} = 7.25$ mm and $l_{\mathrm{s1}} = 1.7$ mm.

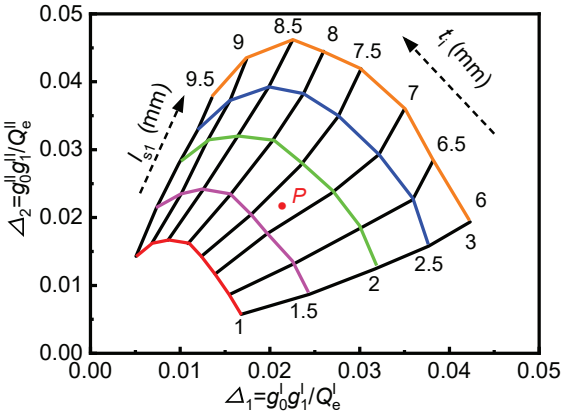

Fig. 3 FBW design graph for the SIW diplexer. Here, $w_{\mathrm{ms}} = 1.29$ mm, $w_{\mathrm{s}} = 0.7$ mm, $w_{\mathrm{i0}} = 3.9$ mm, $w_1 = 12.7$ mm, and $l_1 = 9$ mm. FBW: fractional bandwidth

3.3 Electric field distributions and experimental results

The S-parameters of the diplexer obtained by simulation and measurement are displayed in Fig. 4. The detailed dimensions of the intended diplexer are listed in Table 2. The measurement results of the diplexer are roughly consistent with the simulation results. The center frequencies of the two channels are 10.34 GHz and 13.90 GHz, with −3 dB bandwidths of 590 MHz and 810 MHz, respectively. The minimum insertion losses in the two channels are 2.03 dB and 2.33 dB, respectively. The isolation exceeds 28.1 dB. The measured stopband extends to $2.16f_1$ with a rejection of more than 20 dB. Fig. 5 shows the photograph of the fabricated prototype. The dimensions of the diplexer are 22.5 mm × 17 mm ($1.343\lambda_{\mathrm{g}} \times 1.015\lambda_{\mathrm{g}}$). Figs. 6a and 6b show the electric field distributions in the diplexer at 10.34 GHz (f_1) and 13.90 GHz (f_2), respectively. It proves that

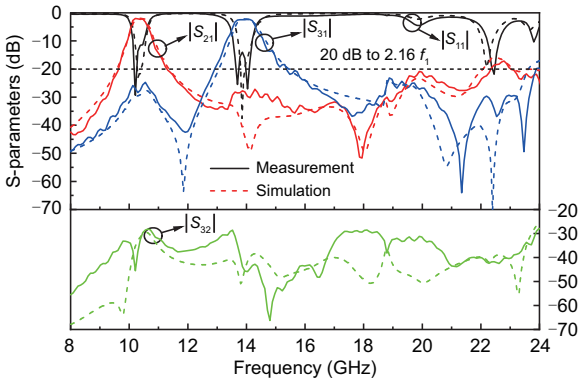

Fig. 4 Comparison between the simulation and measurement results of the proposed diplexer

Table 2 Parameter list

Parameter	Value (mm)	Parameter	Value (mm)
w_{ms}	1.29	l_2^{I}	11.95
w_{s1}	0.7	w_2^{II}	4.9
w_{s2}	0.7	l_2^{II}	7.8
w_{s3}	0.7	t_i	7.25
w_{i0}	3.9	l_{s1}	1.7
w_1	12.7	l_{s2}	1.6
l_1	9	l_{s3}	0.5
w_2^{I}	5.5	w_{c1}	3.9
w_{c2}	3.8		

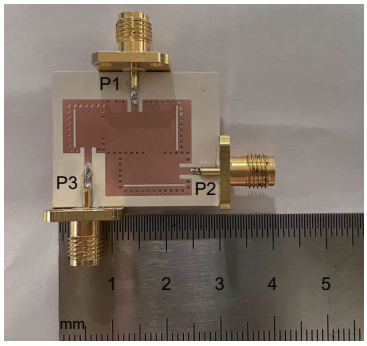

Fig. 5 Photograph of the fabricated prototype

the lower channel is composed of TE_{101} mode in HMSIRCs 1 and 2^{I}, while the upper channel is composed of the TE_{301} mode in HMSIRC 1 and the TE_{101} mode in HMSIRC 2^{II}. Fig. 6c illustrates the electric field distributions in the diplexer at the stopband edge (22.4 GHz). The TE_{301} mode in HMSIRC 2^{I} excites that of HMSIRC 1, resulting in an $|S_{21}|$ peak at 22.5 GHz.

4 Discussions and comparisons

Fig. 7 illustrates the resonant modes of the three HMSIRCs, revealing a staggered higher-order mode distribution in the frequency spectrum. Comparing

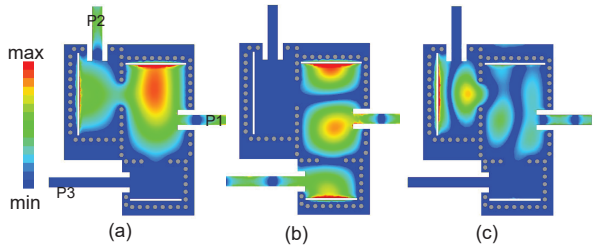

Fig. 6 Electric field magnitude distributions in the diplexer at 10.34 GHz (a), 13.90 GHz (b), and 22.5 GHz (c)

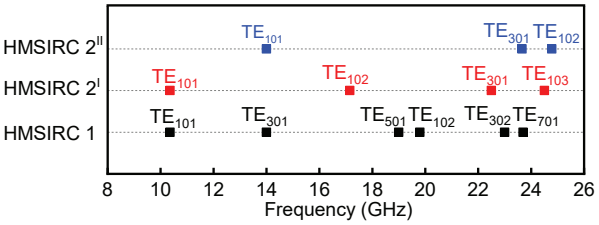

Fig. 7 Frequency spectrum of the initial resonances for the HMSIRCs in the proposed diplexer

Fig. 4 with Fig. 7, we can infer that the peak of $|S_{21}|$ at 22.5 GHz in Fig. 4 is caused by the TE_{301} mode in HMSIRC 2^{I}. Additionally, the $|S_{21}|$ peak of the diplexer at 20 GHz is caused by the TE_{501} and TE_{102} modes in HMSIRC 1. Despite HMSIRC 2^{I} showing a TE_{102} mode response at 17.1 GHz, $|S_{21}|$ does not exhibit a significant peak at this frequency due to the suppression of the coupling window. Therefore, the stopband boundary of the proposed diplexer mainly depends on the first unsuppressed mode in HMSIRC 2^{I}. Table 3 shows the comparison between the proposed diplexer and other SIW diplexers. Compared to the designs in the studies by Zhou et al. (2018a), Iqbal et al. (2019), Xie et al. (2020), Zhou and Wu (2021), and Ma et al. (2023), the diplexer we proposed has a wider stopband. In the study by Liu et al. (2023), various techniques were used to design a wide-stopband diplexer,

Table 3 Comparison with other reported SIW diplexers

Reference	Order	f_1/f_2 (GHz)	−3 dB bandwidth/ FBW (%)	Isolation (dB)	Rejection/ Stopband	IL (dB)	Size (λ_g^2)
Zhou et al. (2018a)	3/3	12/14	4.9/5.65	27	20 dB/1.45f_1	1.34/1.41	2.77
Iqbal et al. (2019)	2/2	10.5/13.5	3.71/1.70	42	20 dB/2f_1	0.80/1.35	2.78
Zhou and Wu (2021)	3/3	3.5/5.0	4.0/3.2	45.8	20 dB/1.7f_1	2.77/2.55	1.62
	4/4	3.5/5.5	3.43/2.55	27.6	20 dB/2.05f_1	3.41/3.40	1.136
Xie et al. (2020)	2/2	10.00/12.25	4.0/3.2	20	24 dB/1.79f_1	2.05/1.65	2.34
	2/2	8/12	3.43/2.55	20	20 dB/2.05f_1	1.84/2.88	1.54
Ma et al. (2023)	3/3	12/14	2.04/2.44	22	20 dB/1.32f_1	2.51/2.19	3.47
	3/3	12/14	3.73/3.99	47	20 dB/2.02f_1	1.39/1.37	3.62
Liu et al. (2023)	4/4	34.95/36.44	1.73/1.39	28.9	20 dB/2.37f_1	4.24/5.10	12.6
This work	2/2	10.34/13.90	5.70/5.83	28.1	20 dB/2.16f_1	2.03/2.33	1.363

yet the circuit area remains large. Our proposed diplexer exhibits superior stopband performance and maintains compactness.

5 Conclusions

A planar SIW diplexer, based on the HMSIW technology, is proposed featuring a wide-stopband and a compact circuit size. Using HMSIRCs in place of whole-mode SIRCs as resonators not only broadens the stopband of the diplexer but also minimizes the circuit area. A second-order prototype centered at 10.34 and 13.90 GHz is fabricated and measured, extending the stopband up to $2.16f_1$ with better than 20 dB rejection level.

Contributors

Ziyu ZHOU designed the research and drafted the paper. Xinqing LEI helped organize the paper. Gang DONG and Zhangming ZHU revised and finalized the paper.

Conflict of interest

All the authors declare that they have no conflict of interest.

Data availability

The data that support the findings of this study are available from the corresponding author upon reasonable request.

References

Bavandpour SK, Roshani S, Pirasteh A, et al., 2021. A compact lowpass-dual bandpass diplexer with high output ports isolation. *AEU-Int J Electr Commun*, 135:153748. https://doi.org/10.1016/j.aeue.2021.153748

Cheng F, Lin XQ, Song KJ, et al., 2013. Compact diplexer with high isolation using the dual-mode substrate integrated waveguide resonator. *IEEE Microw Wirel Compon Lett*, 23(9):459-461. https://doi.org/10.1109/LMWC.2013.2274036

Hong JSG, Lancaster MJ, 2004. Microstrip Filters for RF/Microwave Applications. John Wiley & Sons, New York, USA.

Iqbal A, Tiang JJ, Lee CK, et al., 2019. Tunable substrate integrated waveguide diplexer with high isolation and wide stopband. *IEEE Microw Wirel Compon Lett*, 29(7):456-458. https://doi.org/10.1109/LMWC.2019.2916609

Lai QH, Fumeaux C, Hong W, et al., 2009. Characterization of the propagation properties of the half-mode substrate integrated waveguide. *IEEE Trans Microw Theory Tech*, 57(8):1996-2004. https://doi.org/10.1109/TMTT.2009.2025429

Liu N, Fan CH, Liu XX, et al., 2023. Wide-stopband diplexer with small frequency ratio based on SIW dual-mode resonators for millimeter-wave applications. *IEEE Trans Compon Packag Manuf Technol*, 13(2):284-287. https://doi.org/10.1109/TCPMT.2023.3243204

Ma DD, Zhou K, Xie HW, et al., 2023. Compact or wide-stopband SIW diplexers with high intrinsic isolations based on orthogonal dual modes. *IEEE Trans Circ Syst II Expr Briefs*, 70(1):71-75. https://doi.org/10.1109/TCSII.2022.3208663

Roshani S, Yahya SI, Mezaal YS, et al., 2023. Design of a compact quad-channel microstrip diplexer for L and S band applications. *Micromachines*, 14(3):553. https://doi.org/10.3390/mi14030553

Sieganschin A, Tegowski B, Jaschke T, et al., 2021. Compact diplexers with folded circular SIW cavity filters. *IEEE Trans Microw Theory Tech*, 69(1):111-118. https://doi.org/10.1109/TMTT.2020.3039545

Sirci S, Martínez JD, Vague J, et al., 2015. Substrate integrated waveguide diplexer based on circular triplet combline filters. *IEEE Microw Wirel Compon Lett*, 25(7):430-432. https://doi.org/10.1109/LMWC.2015.2427516

Xie HW, Zhou K, Zhou CX, et al., 2020. Compact SIW diplexers and dual-band bandpass filter with wide-stopband performances. *IEEE Trans Circ Syst II Expr Briefs*, 67(12):2933-2937. https://doi.org/10.1109/TCSII.2020.2992059

Zhou K, Wu K, 2021. Miniaturized diplexers with large frequency ratios based on common half-mode dual-mode SIW junction-cavities. *IEEE Trans Microw Theory Tech*, 69(12):5343-5350. https://doi.org/10.1109/TMTT.2021.3113012

Zhou K, Zhou CX, Wu W, 2017. Resonance characteristics of substrate-integrated rectangular cavity and their applications to dual-band and wide-stopband bandpass filters design. *IEEE Trans Microw Theory Tech*, 65(5):1511-1524. https://doi.org/10.1109/TMTT.2016.2645156

Zhou K, Zhou CX, Wu W, 2018a. Compact SIW diplexer with flexibly allocated bandwidths using common dual-mode cavities. *IEEE Microw Wirel Compon Lett*, 28(4):317-319. https://doi.org/10.1109/LMWC.2018.2805881

Zhou K, Zhou CX, Wu W, 2018b. Dual-mode characteristics of half-mode SIW rectangular cavity and applications to dual-band filters with widely separated passbands. *IEEE Trans Microw Theory Tech*, 66(11):4820-4829. https://doi.org/10.1109/TMTT.2018.2865557

Zhou K, Zhou CX, Wu W, 2020. Compact planar substrate-integrated waveguide diplexers with wide-stopband characteristics. *Int J RF Microw Comput-Aided Eng*, 30(6):e22179. https://doi.org/10.1002/mmce.22179